Research Square

Preprints are preliminary reports that have not undergone peer review.
They should not be considered conclusive, used to inform clinical practice,
or referenced by the media as validated information.

Investigation of Particle Shrinkage, Char Heat Capacity, and Anisotropic Transport Effects on the Pyrolysis of Thermally Thick Wood Spheres

Rachid MECHI

rachid.mechi@isigk.rnu.tn

University of Monastir Institute of Preparatory Studies in Engineering of Monastir: Universite de Monastir Institut Preparatoire aux Etudes d'Ingenieur de Monastir https://orcid.org/0000-0001-7034-1351

Salem Kortas

University of Monastir Institute of Preparatory Studies in Engineering of Monastir: Universite de Monastir Institut Preparatoire aux Etudes d'Ingenieur de Monastir

Rachid Méchi

University of Monastir Institute of Preparatory Studies in Engineering of Monastir: Universite de Monastir Institut Preparatoire aux Etudes d'Ingenieur de Monastir

Habib Farhat

University of Monastir Institute of Preparatory Studies in Engineering of Monastir: Universite de Monastir Institut Preparatoire aux Etudes d'Ingenieur de Monastir

Kamel Halouani

University of Sfax Preparatory Engineering Institute of Sfax: Universite de Sfax Institut Preparatoire aux Etudes d'Engenieur de Sfax

Research Article

Keywords: Biomass pyrolysis, thermally thick particles, particle shrinkage, anisotropic transport, char heat capacity, numerical modeling, intermediate solid kinetics

Posted Date: May 29th, 2026

DOI: https://doi.org/10.21203/rs.3.rs-9595942/v1

License: This work is licensed under a Creative Commons Attribution 4.0 International License.
Read Full License

Investigation of Particle Shrinkage, Char Heat Capacity, and Anisotropic Transport Effects on the Pyrolysis of Thermally Thick Wood Spheres

Salem Kortas[1,2], Rachid Méchi[1,2], Habib Farhat[1,2], Kamel Halouani[3]

[1]University of Sousse, Higher Institute of Applied Sciences and Technology of Sousse, 4002, Sousse, Tunisia
[2]University of Monastir, Laboratory for the Study of Ionized and Reactive Media (EMIR-LR20ES08), Ibn Jazzar Street, Monastir, 5019, Tunisia.
[3]University of Sfax, Preparatory Institute of Engineering Studies of Sfax, Laboratory of Systems Integration and Emerging Energies (SI2E, LR21ES14), 3018, Sfax, Tunisia

Abstract

Accurate prediction of temperature evolution and product yields during the pyrolysis of thermally thick biomass particles remains a significant challenge for reactor design and process optimization. This study examines the coupled influence of particle shrinkage and char heat capacity correlations on mass loss, product yields, and intraparticle temperature in wood spheres. A transient two-dimensional model is developed for a 25.4 mm diameter particle exposed to a constant reactor wall temperature of 736 K. The model combines an intermediate solid kinetic scheme, Darcy type volatile transport, conversion dependent properties, and anisotropic thermal conductivity and permeability based on literature data. Three char heat capacity correlations are implemented and assessed against experimental center temperature profiles and final char yields. Among them, a linear correlation provided the closest overall agreement, accurately reproducing both the endothermic plateau and the peak temperature. The best agreement with experiments is obtained for a radial shrinkage factor of 10%. Increasing shrinkage shifts the temperature peak to earlier times and progressively shortens the plateau period, which disappears for shrinkage levels above 30%. In addition, neglecting anisotropic transport properties leads to unrealistically rapid internal heating. The results demonstrate that reliable pyrolysis modeling of large biomass particles requires consistent treatment of thermophysical properties together with structural evolution effects.

Keywords: Biomass pyrolysis; thermally thick particles; particle shrinkage; anisotropic transport; char heat capacity; numerical modeling; intermediate solid kinetics

List of symbols

A_i	Pre-exponential factor of reaction i [s^{-1}]
B	Permeability tensor [m^2]
B_{eff}	Effective permeability [m^2]
B_w, B_c	Wood and char permeability [m^2]
Bi	Biot number [–]
c_p	Specific heat capacity [J kg^{-1} K^{-1}]
d_o	Initial particle diameter [m]
d_{eff}	Effective pore diameter [m]
d_w, d_{char}	Wood and char pore diameter [m]
E_i	Activation energy of reaction i [J mol^{-1}]
f_{radial}	Radial shrinkage factor [–]
h	Convective heat transfer coefficient [W m^{-2} K^{-1}]
k_i	Rate constant of reaction i [s^{-1}]
k_t, k_g, k_{is}, k_{g2}, k_{c2}, k_{char}	Reaction kinetic constants [s^{-1}]
M_g	Molar mass of non-condensable gas [kg mol^{-1}]
M_t	Molar mass of tar [kg mol^{-1}]
Nu	Nusselt number [–]
p	Gas pressure [Pa]
Pr	Prandtl number [–]
$\dot{Q}_{chem}$	Volumetric chemical heat source term [W m^{-3}]
R	Universal gas constant [J mol^{-1} K^{-1}]
Re	Reynolds number [–]
r,z	Radial and axial coordinates [m]
r_p	Particle radius [m]
$\dot{m}_w$	Volume averaged virgin wood conversion rate [kg m^{-3} s^{-1}]
$\dot{S}_f$	Volatile mass source term [kg m^{-3} s^{-1}]
t	Time [s]
T	Temperature [K]
u (u_r, u_z)	Gas velocity vector [m s^{-1}]

u_r, u_z	Radial and axial gas velocities [m s^{-1}]
$u_{radial,\ shrinkage}$	Radial shrinkage velocity [m s^{-1}]
Y_{char}	Final char yield [wt.%]

Greek letters

α_{eff}	Effective thermal diffusivity [m^2 s^{-1}]
ΔH_i	Enthalpy of reaction i [J kg^{-1}]
ε	Porosity [–]
ε_o	Initial porosity [–]
ε_{rad}	Emissivity [–]
η	Degree of pyrolysis (local conversion) [–]
λ	Thermal conductivity [W m^{-1} K^{-1}]
λ_{eff}	Effective thermal conductivity [W m^{-1} K^{-1}]
λ_{bulk}	Bulk solid thermal conductivity [W m^{-1} K^{-1}]
λ_f	Gas phase thermal conductivity [W m^{-1} K^{-1}]
λ_{rad}	Radiative contribution to thermal conductivity [W m^{-1} K^{-1}]
μ	Dynamic viscosity [kg m^{-1} s^{-1}]
ρ	Density [kg m^{-3}]
σ	Stefan–Boltzmann constant [W m^{-2} K^{-4}]

Subscripts

0	Initial value
c	center
char	Char
c_2	Secondary char from tar conversion
eff	Effective
f	Fluid / pore gas
g	Non-condensable gas
g_2	Secondary gas from tar conversion
is	Intermediate solid
rad	Radiation
radial	radial direction

s	Surface
t	Tar
w	Wood
wall	Reactor wall

Abbreviations

ALE	Arbitrary Lagrangian–Eulerian,
BDF	Backward differentiation formula
LTE	Local Thermal Equilibrium
SEM	Scanning Electron Microscopy

1. Introduction

The thermochemical conversion of lignocellulosic biomass is an important industrial route for the production of sustainable heat, power, fuels, chemicals, and carbonaceous materials. Among the available conversion technologies, pyrolysis is widely used to produce char, bio-oil, and non-condensable gas, and its performance depends strongly on the interaction between operating conditions and biomass properties. For thermally thick biomass particles, conversion is governed by coupled heat transfer, mass transport, and chemical reactions occurring within a porous and deforming solid structure [1–3]. Accurate assessment of these interactions is therefore essential for process design, reactor performance prediction, and industrial process optimization [1, 2, 4].

Early modeling studies established the fundamental role of transport limitations during biomass pyrolysis. Initial works incorporated internal heat transfer together with reaction kinetics, providing the basis for later coupled transport reaction models [5, 6]. More relevant analyses showed that, for large particles under slow and intermediate heating conditions, the overall conversion may be controlled by heat transfer rather than by intrinsic kinetics, as formalized in [7]. Later, experimental and numerical studies confirmed that resolving internal temperature gradients in thermally thick particles, is necessary to reproduce temperature profiles, mass loss, and product yields [8–12].

Structural changes during pyrolysis, particularly particle shrinkage, have been identified as a decisive factor influencing internal heat transfer. Di Blasi [13] introduced shrinkage particle modeling, showing that reducing particle size decreases the thickness of the insulating char layer and enhances heat penetration. Later analogous works demonstrated that shrinkage can significantly reduce conversion time and alter volatile release patterns [14–16]. Bellais et al. [17] revealed the sensitivity of model predictions to shrinkage assumptions, while [18] showed that shrinkage affects both heat transfer and reaction kinetics. Additional studies confirmed that shrinkage interacts with operating conditions to influence product yields and conversion behavior [19]. Experimental observations have also reported transient swelling, followed by contraction during pyrolysis [20], and recent computational studies indicate that shrinkage affects both particle scale processes and reactor hydrodynamics [21].

Particle geometry further influences pyrolysis behavior. Spherical particles, characterized by a low surface area to volume ratio, exhibit higher internal thermal resistance compared to other shapes [22]. Particle size also affects devolatilization kinetics and fast pyrolysis product yields, since heat transfer and vapor residence times vary with particle dimensions and shape. Suriapparao and Vinu [23] showed

that particle size, shape, composition, heating rate, and residence time must be considered jointly to support process scale up. Experimental investigations on large wood spheres have revealed distinct thermal features, including a temperature plateau followed by a rapid temperature rise at the particle center [9, 24]. These observations highlight the importance of accurately representing internal transport phenomena in thermally thick particles.

In addition to geometry and shrinkage, the anisotropic nature of wood significantly affects transport processes. Due to its fibrous cellular structure, direction dependent thermal conductivity and permeability must be considered [25]. Di Blasi [26] demonstrated that anisotropy significantly redistributes the balance between conductive and convective heat transfer. Consequently, internal heating cannot be interpreted through thermal conductivity alone; the lower permeability across the grain restricts volatile transport and increases internal pressure, thereby modifying heat transfer within the material. Further studies confirmed that neglecting anisotropy leads to inaccurate predictions of conversion time, temperature fields, gas flow, and pressure driven transport effects [2, 27, 28]. In particular, conditions under which anisotropy must be considered for accurate conversion time prediction were identified in [27]. Sánchez et al. [28] showed that axial and radial conductivity and permeability play a major role in predicting conversion time and product yields, with anisotropy becoming especially important in thermally thick particles [2]. More advanced anisotropic particle models have therefore been developed to improve prediction of intraparticle temperature fields, gas flow behavior, and product yields [28–30].

Martí-Rosselló et al. [31] conducted a comparative study between one-dimensional and three-dimensional models for biomass pyrolysis. They found that one-dimensional models are efficient for predicting final char yield, whereas three-dimensional models are required to accurately predict transient mass loss rates and internal spatial variations of char porosity.

Recent studies show that models must combine directional transport properties with wood biomass deformation. Shi et al. [32] developed a three-dimensional finite element model including transport, kinetics, and particle size reduction effects, showing that shrinkage affects volatile residence time, internal transport, and char formation.

Experimental investigations provide complementary evidence for anisotropic dimensional structural evolution. Caposciutti et al. [33] quantified anisotropic swelling and shrinkage using image analysis, while [34] used Scanning Electron Microscopy (SEM) and X-ray Computed Tomography (X-ray CT) to reveal anisotropic pore development and the influence of heating rate. Additional studies have shown

that fiber orientation affects thermal conductivity, thermal degradation behavior, and moisture transport. In particular, a three-dimensional anisotropic degradation model for wood was developed in [35], while, direction dependent thermal conductivity and heat capacity were measured in [36]. Fiber orientation also influences temperature fields and decomposition stages during pyrolysis [30]. Moreover, direction dependence moisture transport in wood supported by X-ray CT was demonstrated in [37]. These findings indicate that realistic biomass pyrolysis models should account simultaneously for anisotropy, structural transformation, and multiphase transport.

The determination of pyrolysis kinetics is generally based on thermogravimetric analysis (TGA), which provides mass loss data under controlled heating conditions. This approach is used to estimate apparent Arrhenius law parameters and to evaluate multistep reaction schemes for biomass [38, 39] and other feedstocks [40].

The selection of an appropriate kinetic scheme is essential for predicting pyrolysis behavior. Conventional global or competitive reaction models often fail to reproduce the temperature plateau and exothermic peak observed thermally thick particles [2, 9]. To address this limitation, intermediate solid approaches and more detailed multistep kinetic schemes have been developed. Park et al. [9], attributed the late temperature peak to exothermic decomposition of an intermediate solid, while next multiscale kinetic frameworks improved predictions of temperature fields and product yields under thermally thick conditions [12, 38, 39, 41].

In addition to kinetics, the selection of thermophysical property correlations is critical for achieving accurate predictions. In particular, the heat capacity of char governs the thermal inertia of the solid matrix and strongly influences temperature evolution during pyrolysis. Various temperature dependent correlations have been used in particle scale models [2, 6, 18, 42, 43]. However, their influence on model predictions, especially when combined with shrinkage and anisotropic transport, remains insufficiently investigated.

Despite substantial progress in biomass pyrolysis modeling, the combined influence of particle shrinkage, anisotropic transport properties, and alternative char heat capacity correlations is not well quantified for large thermally thick particles. Many previous studies have addressed these effects separately, whereas their coupled impact has not been systematically evaluated for spherical geometries characterized by significant internal thermal resistance. Recent reviews have also emphasized the need for integrated modeling approaches that account for interactions among transport phenomena, solid matrix transformations, and reaction kinetics while maintaining physical consistency [2, 3, 44].

Therefore, this work develops a transient two-dimensional model to simulate the pyrolysis of a large wood sphere under thermally thick conditions. The model incorporates particle shrinkage, anisotropic thermal conductivity and permeability, an intermediate solid kinetic scheme, and alternative char heat capacity correlations. Model predictions are evaluated against published center temperature profiles and char yield data to identify the most suitable property representation. The objective is to clarify the relative importance of these coupled effects and improve the predictive capability of particle scale pyrolysis models for sustainable energy applications.

2. Physical model and governing equations

2.1 Physical model

Figure 1 illustrates the spherical particle and the representation of directional transport properties associated with the anisotropic structure of wood.

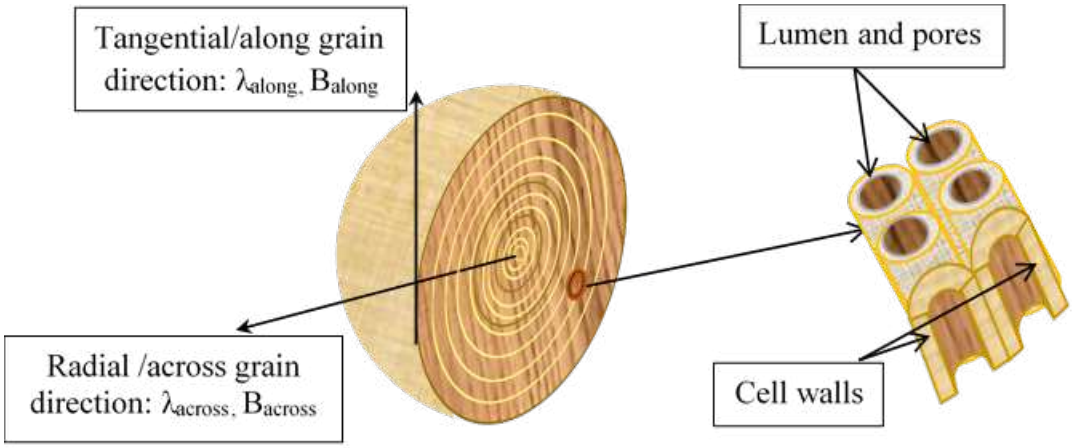


Fig. 1 Schematic representation of the spherical particle and the directional transport properties inherited from the wood structure.

A dry spherical maple wood particle with an initial diameter of 25.4 mm is considered. The particle is exposed to a constant reactor wall temperature of 736 K, corresponding to the experimental conditions reported in [9]. The system operates under inert conditions, and the present thermochemical model is formulated in the transient regime. The spherical geometry is selected to isolate internal transport effects while avoiding geometric complexities associated with cylindrical or irregular particles.

The present approach assumes local thermal equilibrium (LTE) between the solid matrix and the pore gas. The governing equations are expressed in a two-dimensional axisymmetric coordinate system

and anisotropic effects are incorporated through direction dependent effective thermal conductivity and permeability. The particle undergoes shrinkage during conversion, with a corresponding evolution of porosity. Volatile transport within the porous structure is modeled using a Darcy–Brinkman formulation.

Table 1 summarizes the main operating conditions and modeling assumptions.

Table 1. Principal operating conditions and assumptions used throughout the simulations.

Parameters	Value / description
Particle geometry	Sphere
Initial wood density $\rho_{w,o}$	630 kg m^{-3}
Initial diameter d_o	25.4 mm
Initial temperature	300 K
Reactor temperature	736 K
Atmosphere	Inert
Model type	Transient spherical particle model
Thermal equilibrium	Local equilibrium between solid and pore gas
Shrinkage range	0, 5, 8, and 10% radial shrinkage; extended sensitivity to higher values for selected cases
Kinetic framework	Intermediate solid scheme in [9]
Transport representation	Conversion dependent conductivity, permeability, porosity, and volatile flow

2.2 Governing equations

The governing equations are solved under local thermal equilibrium between the solid matrix and pore gas.

Kinetic Model

The wood pyrolysis reaction network follows the intermediate solid mechanism proposed by [9]:

- Wood → Tar + Gas (endothermic)
- Wood → Intermediate Solid (endothermic)
- Tar → Char + Gas (exothermic)
- Intermediate solid → Char (exothermic)

The temperature dependent reaction rate for each step in the kinetic scheme follows the Arrhenius law:

$$k_i = A_i \exp\left(-\frac{E_i}{RT}\right) \quad (1)$$

The values of the kinetic parameters and the heats of pyrolysis reactions used in the present model are listed in Table 2.

Table 2. Kinetic parameters values for pyrolysis primary and second reactions.

Parameters	E_i (kJ mol^{-1})	A_i (s^{-1})	ΔH_i (kJ kg^{-1})
k_t (s^{-1})	148[a]	1.08×10^{10}[a]	117[b]
k_g (s^{-1})	152[a]	4.38×10^{9}[a]	117[b]
k_{is} (s^{-1})	111.7[a]	2.3×10^{6}[c]	117[b]
k_{g2} (s^{-1})	108[a]	4.28×10^{6}[a]	-42[a]
k_{c2} (s^{-1})	108[a]	1.00×10^{5}[a]	-42[a]
k_{char} (s^{-1})	112.7[a]	1.48×10^{10}[b]	-296[b]
	a [9]	b [45]	

Porosity Evolution

Porosity increases with conversion as solid material is decomposed into char and volatiles:

$$\varepsilon = 1 - \frac{\rho_w}{\rho_{w,o}}(1 - \varepsilon_o) \tag{2}$$

where ρ_w and $\rho_{w,o}$ denote the local and initial wood density respectively, and $\varepsilon_o = 0.4$ is the initial porosity [9].

Energy Conservation

The two-dimensional transient energy balance is written as:

$$\left(\rho C_p\right)_{\text{eff}} \frac{\partial T}{\partial t} + \nabla \cdot (-\boldsymbol{\lambda}_{\text{eff}} \nabla T) + \rho_f C_{p,f} (\mathbf{u} \cdot \nabla) T = \dot{Q}_{chem} \tag{3}$$

The axisymmetric assumption enables the modeling of direction dependent heat transport properties. Accordingly, the effective thermal conductivity is expressed in tensorial form, accounting for the along-grain and across-grain directions:

$$\boldsymbol{\lambda}_{eff} = \begin{bmatrix} \lambda_{r,eff} & 0 \\ 0 & \lambda_{z,eff} \end{bmatrix} \tag{4}$$

The chemical heat source term is given by:

$$\dot{Q}_{chem} = -\rho_w (k_{\text{t}} \Delta H_{\text{t}} + k_{\text{g}} \Delta H_{\text{g}} + k_{\text{is}} \Delta H_{\text{is}}) - \rho_{is} k_{\text{char}} \Delta H_{\text{char}} - \rho_f k_{g2} \Delta H_{g2} - \rho_f k_{c2} \Delta H_{c2} \tag{5}$$

This formulation accounts for both endothermic and exothermic reactions within the intermediate solid kinetic scheme.

Effective Thermophysical Properties

The effective volumetric heat capacity is defined as:

$$\left(\rho c_p\right)_{eff} = \rho_w c_{p,w} + \rho_{is} c_{p,is} + \rho_c c_{p,char} + \varepsilon \rho_g c_{p,g} + \varepsilon \rho_t c_{p,t} \tag{6}$$

Three correlations for char heat capacity are considered and evaluated:

$$c_{p,char}^{(1)} = 420 + 2.09\,T + 6.85 \times 10^{-4}\,T^2 \tag{7a}$$

$$c_{p,char}^{(2)} = 1003 + 2.09\,(T - 271) \tag{7b}$$

$$c_{p,char}^{(3)} = 1390 + 0.36\,T \tag{7c}$$

These expressions are taken from [8], [10, 18], and [46], respectively. The effective thermal conductivity λ_{eff} is given by:

$$\lambda_{eff} = (1 - \varepsilon)\,\lambda_{bulk} + \varepsilon\,\lambda_f + \lambda_{rad} \tag{8}$$

with radiative contribution:

$$\lambda_{rad} = 4\sigma d_{eff}\,\varepsilon_{rad}\,T^3 \tag{9}$$

The bulk thermal conductivity varies using a linear interpolation between the properties of virgin wood and char:

$$\lambda_{bulk} = (1 - \eta)\,\lambda_w + \eta\,\lambda_{char} \tag{10}$$

where the degree of pyrolysis is:

$$\eta = 1 - \frac{\rho_w + \rho_{is}}{\rho_{w,o}} \tag{11}$$

Table 3 summarizes the thermophysical and anisotropic transport properties for wood and the different pyrolytic products used in the model.

Table 3. Thermophysical and anisotropic transport properties for wood and different pyrolytic products used in the model.

Specific heat (J kg^{-1} K^{-1})		
wood ($c_{p,w}$)	$1500 + 1.0 \times T$	[8]
char ($c_{p,char}$)	$420 + 2.09 \times T + 6.85 \times 10^{-4} \times T^2$	[8]
	$1003 + 2.09 \times (T - 271)$	[18]
	$1490 + 0.36 \times (T)$	[46]
tar (c_t)	$-100 + 4.4 \times T - 1.57 \times 10^{-3} \times T^2$	[8]
gas (c_g)	$770 + 0.629 \times T - 1.91 \times 10^{-4} \times T^2$	
N_2(c_{N_2})	$950 + 0.188 \times T$	
Pore size		
wood (d_w) (μm)	40	[9]
char (d_{char}) (μm)	400	
initial porosity (ε_o)	0.4	
Emissivity		
wood ($\varepsilon_{rad,\,w}$)	0.7	[9]

char ($\varepsilon_{rad,\ char}$)	0.92	
Thermal conductivity (W m^{-1} K^{-1})		
char-along grain ($\lambda_{char,\ along}$)	0.105	[9]
char-across grain ($\lambda_{char,\ across}$)	0.071	
mixture ($\lambda_{mixture}$)	0.0258	
wood-along grain ($\lambda_{w,\ along}$)	$2.8 \times \lambda_{w,across}$	[32]
wood-across grain ($\lambda_{w,\ across}$)	$\frac{\rho_{w,o}}{\rho_{water}}(0{,}1941 + 0{,}004064 \times M + 0{,}01864)$	
Permeability (m^2)		
wood - along grain ($B_{w,\ along}$)	10^{-11}	[32]
wood - across grain ($B_{w,\ across}$)	10^{-14}	
char - along grain ($B_{char,\ along}$)	5×10^{-11}	
char - across grain ($B_{char,\ across}$)	5×10^{-12}	
viscosity (μ) (kgm^{-1} s^{-1})	3×10^{-5}	[9]
Molar mass (kg mol^{-1})		
gas (M_g)	0.038	[8]
tar (M_t)	0.11	

2.3 Mass and momentum conservation

Species Conservation

As thermal degradation progresses, the wood particle is converted into a new solid phase and a volatile mixture. The mass conservation equations for the solid matrix components (wood, intermediate solid, char) and volatiles products (tar and non-condensable gas) are expressed as follows:

$$\begin{cases} \frac{\partial \rho_w}{\partial t} = -(k_{\mathrm{t}} + k_{\mathrm{g}} + k_{\mathrm{is}})\rho_w \\ \frac{\partial \rho_{is}}{\partial t} = k_{\mathrm{is}}\rho_w - k_{\mathrm{char}}\rho_{is} \\ \frac{\partial \rho_{char}}{\partial t} = k_{\mathrm{is}}\rho_{is} + k_{c2}\rho_t \\ \frac{\partial \rho_t}{\partial t} + \nabla \cdot (\rho_t \mathbf{u}) = k_{\mathrm{t}}\rho_w - k_{g2}\rho_t - k_{c2}\rho_t \\ \frac{\partial \rho_g}{\partial t} + \nabla \cdot \left(\rho_g \mathbf{u}\right) = k_{\mathrm{g}}\rho_w + k_{g2}\rho_t \end{cases} \quad (12)$$

Gas Phase Transport

The transport of volatiles within the porous structure is governed by the gas-phase mass conservation equation:

$$\frac{\partial(\varepsilon\rho_f)}{\partial t} + \nabla \cdot \left(\varepsilon\rho_f \mathbf{u}\right) = \dot{S}_f \quad (13)$$

Mass conservation between solid consumption and volatile production is ensured through the total volatile source term:

$$\dot{S}_f = -(k_g \rho_w + k_{g2} \rho_t) \tag{14}$$

The gas velocity is computed using the Brinkman equation:

$$\frac{\rho_f}{\varepsilon}\frac{\partial u}{\partial t} + \mu \boldsymbol{B}_{\boldsymbol{eff}}^{-1} \cdot u = -\nabla p + \nabla \cdot \left[\mu_{eff}(\nabla u + (\nabla u)^T)\right] \tag{15}$$

where the anisotropic effective permeability in the axisymmetric model is defined by the following tensor:

$$\boldsymbol{B}_{\boldsymbol{eff}}^{-1} = \begin{bmatrix} \frac{1}{B_{r,eff}} & 0 \\ 0 & \frac{1}{B_{z,eff}} \end{bmatrix} \tag{16}$$

The directional components of the effective permeability are determined, as a function of the local degree of conversion:

$$B_{i,eff} = (1-\eta)\, B_{i,w} + \eta\, B_{i,char} \qquad (i = r, z) \tag{17}$$

Boundary Conditions

At the particle surface, the following thermal boundary condition below is applied:

$$-\lambda_{eff} \left.\frac{\partial T}{\partial r}\right|_{r=r_p} = h\,(T_{wall} - T_s) + \sigma\, \varepsilon_{rad}\,(T_{wall}^4 - T_s^4) \tag{18}$$

The Biot number is defined as follows:

$$Bi = \frac{h\, r_p}{\lambda_{eff}} \tag{19}$$

The Biot number remains significantly greater than unity, indicating that the biomass particle exhibits thermally thick behavior throughout the conversion process [7].

Shrinkage Model

Particle shrinkage is modeled using a moving boundary approach:

$$u_{radial,\ shrinkage} = -f_{radial} \cdot \frac{\dot{m}_w}{m_{w,0}} \cdot \frac{d_0}{2} \tag{20}$$

The radial shrinkage factor, f_{radial} represents the relative reduction in particle radius (0–30%) and $\dot{m}_w$ denotes the biomass decomposition rate [32].

Numerical Implementation

The governing equations were implemented using a fully coupled transient finite element formulation in COMSOL Multiphysics. The problem was solved in a two-dimensional axisymmetric domain representing the spherical particle, enabling incorporation of anisotropic thermal conductivity and permeability while maintaining computational efficiency.

Particle shrinkage was described using the Deformed Geometry (Arbitrary Lagrangian–Eulerian, ALE) method. The computational domain contracts dynamically according to the shrinkage velocity defined in Eq. (20), ensuring that the external boundary remains consistent with the local biomass conversion rate throughout pyrolysis.

Spatial discretization employed mapped quadrilateral elements in the axisymmetric (r, z) domain. A non-uniform mesh with progressive refinement toward the particle surface was adopted to resolve the steep gradients in temperature, conversion, and volatile concentration associated with the formation of the outer char layer. The final mesh contained approximately 2×10^4 elements, providing adequate resolution of both thermal and reaction fronts.

Time integration was performed using an implicit backward differentiation formula (BDF) scheme with adaptive time stepping. The resulting nonlinear algebraic system was solved using a fully coupled newton based procedure with automatic damping, improving convergence during strongly nonlinear stages, particularly near the exothermic temperature peak.

Axisymmetric boundary conditions were imposed along the centerline. At the external surface, heat transfer obeys to the combined convective and radiative boundary condition given in Eq. (18). The moving boundary was handled consistently through the ALE formulation.

Mesh independence was verified by progressive refinement until variations in predicted center temperature and overall conversion were below 1%. Additional time step sensitivity tests confirmed that the adaptive BDF scheme provided stable and accurate solutions over the full simulation interval of 0–600 s.

Figure 2 shows the computational mesh used in the simulations.

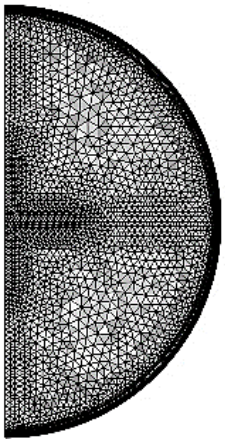


Fig. 2 Finite element mesh used for the spherical particle simulations.

3. Results and discussion

This section analyzes the coupled heat and mass transfer behavior of a 25.4 mm spherical maple wood particle subjected to pyrolysis in a hot vertical flow reactor with a constant wall temperature of 736 K. Particular attention is given to the effects of temperature dependent char heat capacity, particle shrinkage, and anisotropic transport properties on temperature evolution, conversion behavior, and products yields. The discussion follows the temporal progression of the process and combines global performance indicators with examination of the internal temperature, pressure, and flow fields.

3.1 Thermal response and characteristic phases

The temporal evolution of the particle center temperature, shown in Figs. 3 and 4, displays the characteristic three stage heating behavior of biomass pyrolysis. These stages are consistent with the intermediate solid kinetic mechanism reported by [9]. During the initial heating period, extending approximately from 0 to 150 s, the center temperature increases monotonically from ambient conditions to the onset of devolatilization. This stage is boosted basically by conductive heat transfer through the solid matrix, as described by Eq. (3). The effective thermal diffusivity evolves continuously due to both the progressive conversion from wood to char and the temperature dependence of thermophysical properties. The inclusion of anisotropic thermal conductivity enhances radial heat transfer and accelerates internal heating compared to isotropic assumptions. This is well confirmed by several studies on thermally thick particles. They showed that directional transport effects become significant once internal gradients develop. Anisotropy alters the coupled conductive, convective, and pressure driven transport processes, leading to non-equivalent temperature fields along and across the grain [26].

Moreover, anisotropy affects the internal temperature distribution, gas velocity field, and local heating rates particularly in thermally thick particles, where an outer heated layer develops while the core remains transport limited for a significant portion of the process [2, 27, 30]. Direction dependent transport properties influence center heating not only through conduction but also indirectly by modifying volatile release, gas flow, and the associated feedback of off-gassing on the incoming heat flux.

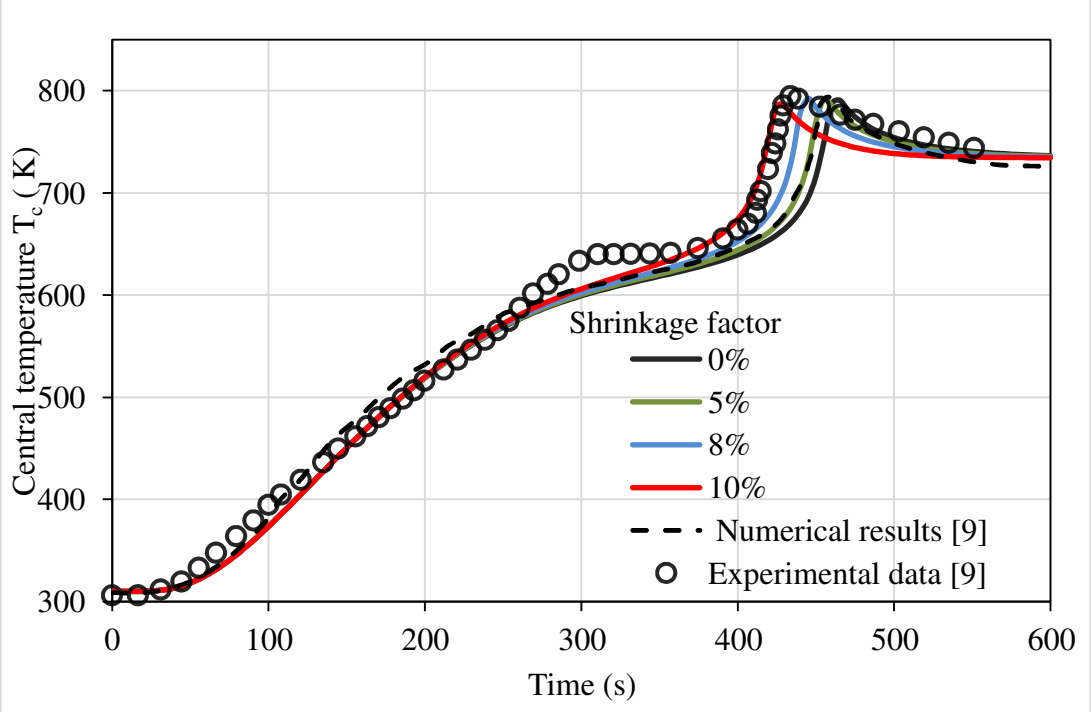


Fig. 3 Effect of shrinkage factor on center temperature T_c, using the char specific heat capacity correlation from [9].

The present model accounts for the directional dependence of both thermal conductivity and the gas permeability of the wood particle, using permeability data from [8, 9, 32]. Although the influence of conductivity anisotropy on center temperature prediction is generally secondary for thermally thick spheres, anisotropic permeability can redirect volatile flow from radial toward longitudinal directions, thereby reducing convective counterflow opposing the incident heat flux and accelerating overall conversion in agreement with [27]. The timescale of the initial heating stage remains consistent, indicating that advancement of the thermal front is undertaken essentially by diffusive heat transport, as expected for the thermally thick regime [7].

As the temperature reaches the range of active devolatilization, a quasi-steady plateau is established between approximately 150 and 300 s. In this regime, the temperature stabilizes near 610–640 K as a result of the balance between conductive heat input and highly endothermic primary pyrolysis reactions. Using the correlation proposed by [9], the predicted plateau duration remains close to 150 s, consistent with experimental observations. When the alternative correlation used from [18] is employed, as illustrated in Fig. 4, the plateau is slightly extended. This behavior reflects an increase in effective heat capacity, which enhances the thermal inertia of the char layer and requires additional energy to sustain further temperature rise.

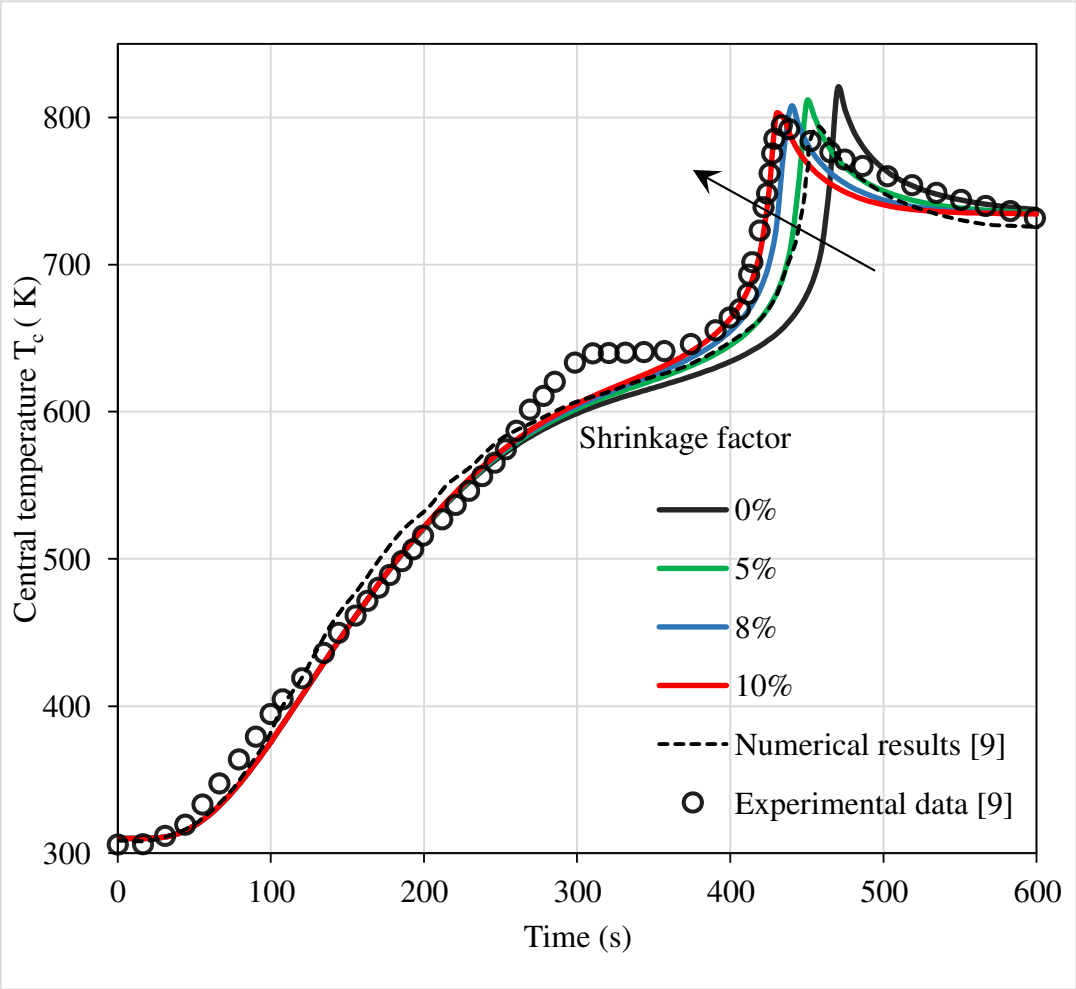


Fig. 4 Effect of shrinkage factor on the spherical particle central temperature T_c, using the char specific heat capacity correlation (Eq. 7b, [18]).

At later times, typically beyond 300 s, the temperature evolution is dominated by the exothermic decomposition of the intermediate solid. This stage is characterized by a temperature thermal peak during which the particle center temperature surpasses the reactor wall temperature. Using the reference

correlation, the predicted center temperature exceeds the wall temperature by approximately 30 to 35 K, in good agreement with experimental measurements reported in [9]. In contrast, the use of an alternative heat capacity correlation reduces the peak magnitude by about 20–22 K, as shown in Fig. 4. This reduction is attributed to the higher heat capacity at elevated temperatures, which increases the thermal capacitance of the char matrix and enhances its ability to absorb and buffer the heat released during exothermic reactions.

The process remains within the thermally thick regime as significant internal temperature gradients persist throughout conversion and the particle center does not respond quasi-isothermally to the external boundary conditions. When internal and external to heat transfer resistances are of comparable magnitude, the reaction zone tends to extend over a larger portion of the particle rather than being confined to a narrow moving front [14, 15]. The predicted plateau near 610–640 K and the subsequent temperature peak at the center are in good qualitative agreement with observations reported for large biomass particles. The plateau corresponds to an endothermic stage, whereas the later peak reflects an exothermic stage associated with intermediate solid decomposition, particularly as described in [9, 47]. At the same time, the plateau plus peak sequence has also been attributed to secondary interactions between volatiles and char [6], indicating that its detailed mechanistic origin remains subject to discussion.

. The internal convection contributes to lowering the predicted center temperature by transporting enthalpy outward, whereas particle shrinkage tends to increase it by retaining a larger fraction of internally generated heat [11]. Overall, the literature consistently reports the existence of the plateau plus peak pattern, although discrepancies remain regarding its precise reaction level origin [6, 9, 11, 47]. By coupling anisotropic transport properties alongside the intermediate solid mechanism, the present model provides additional insight into the complex coupling between transport phenomena and reaction kinetics.

3.2 Influence of particle shrinkage

Particle shrinkage introduces a direct coupling between geometry and transport processes. As the particle contracts during conversion, the conduction path length decreases while the effective thermal mass of the char layer is reduced. These combined effects lead to a measurable modification of the thermal response. Increasing the shrinkage factor from 0 to 10 % results in a shorter plateau duration and an earlier occurrence of the temperature peak. At the same time, the peak magnitude increases due to the reduced capacity of the shrinkage particle to buffer the heat released during exothermic reactions.

A quantitative analysis of the numerical results reveals that both the peak temperature T_{peak} and the time t_{peak} at which it occurs vary linearly with the shrinkage factor within the physically realistic range. The following correlations were obtained by least squares regression:

$$t_{\mathrm{peak}} = -392.1 \times f_{radial} + 470.0 \quad \text{(s)}, \quad R^2 = 0.997 \tag{21a}$$

$$T_{peak} = -159.4 \times f_{radial} + 819.1 \quad \text{(K)}, \quad R^2 = 0.98 \tag{21b}$$

These relationships indicate that shrinkage accelerates the process while simultaneously reducing the effective thermal buffering capacity. This behavior is consistent with the dependence of characteristic time scales on particle size in the thermally thick regime [7, 13, 15, 16]. However, extending the shrinkage beyond approximately 10% leads to thermal profiles not supported by experimental observations.

3.3 Effect of char heat capacity correlation

The choice of char heat capacity correlation has a strong impact on the predicted thermal behavior. The correlation adopted from [9] provides a balanced representation of both the plateau and the temperature peak. The alternative formulation from [18], illustrated in Fig. 4, increases the plateau duration while reducing this peak magnitude, leading to improved agreement with experimental trends. This confirms that an accurate description of the temperature dependence of char heat capacity is essential for correctly resolving the energy balance.

In contrast, the correlation reported in [46] produces distorted thermal dynamics, characterized by excessively temperature peaks. This behavior arises from the relatively high baseline values of the char heat capacity (approximately 1390–1502 J kg^{-1} K^{-1} over the considered temperature range). The resulting reduction in thermal diffusivity within the char layer limits outward heat dissipation, increases the residence time of the exothermic intermediate solid within the conversion zone, and promotes excessive energy accumulation before it can be released. This discrepancy likely originates from the fact that the correlation was developed for highly carbonized char typical of gasification conditions, which differs significantly from the properties of char formed during pyrolysis. Its direct application therefore leads to an inaccurate representation of heat accumulation during the exothermic stage.

3.4 Role of anisotropic transport properties

The incorporation of anisotropic transport properties improves the physical realism of the model and influences all stages of the process [9]. In spherical geometry, the directional conductivities are often homogenized using an effective isotropic representation given by:

$$\lambda_{eff,\ sphere} = \frac{\lambda_{\text{along}} + 2\lambda_{\text{across}}}{3} \tag{22}$$

This equation accounts for the structural anisotropy of wood while preserving a simplified radial framework. However, in the present two-dimensional model, a tensor formulation (Eq. (4)) is employed to explicitly represent direction dependent thermal conductivity. This tensorial approach enhances heat transfer during the initial heating stage and contributes to a more accurate prediction of the temperature field. It also tends to shorten the plateau duration and mitigate the peak temperature by facilitating heat dissipation through the char layer. These effects are consistent with previous studies indicating that neglecting anisotropy can lead to significant deviations in temperature field prediction, heating rate distribution, and conversion behavior [2, 9, 28, 30].

Permeability anisotropy governs the internal transport of volatile species, thereby coupling mass and heat transfer. Preferential flow along high permeability directions leads to non-uniform pressure distributions and affects the residence time of volatiles within the particle. As a result, the interaction between gas flow and thermal fields becomes strongly coupled, influencing both local temperature profiles and the extent of secondary reactions [2, 26, 27, 30, 32, 48].

3.5 Mass loss evolution

The evolution of the normalized solid mass fraction, shown in Fig. 5, indicates that shrinkage has a limited influence on the overall conversion rate. All simulated cases remain in close agreement with the experimental data reported by [9], and the differences between shrinkage scenarios are small. This confirms that, under thermally thick conditions, shrinkage has at most a secondary effect on overall conversion time compared with the dominant role of heat transfer [14, 15, 18]. The conversion rate is stimulated primarily by heat transfer rather than by intrinsic reaction kinetics. This dominance confirms that internal thermal resistance controls the process which is consistent with the Biot number range identified earlier [7]. Under such conditions, the conversion rate is mainly by the propagation of the thermal field through the particle rather than by intrinsic kinetics alone [7, 14, 18].

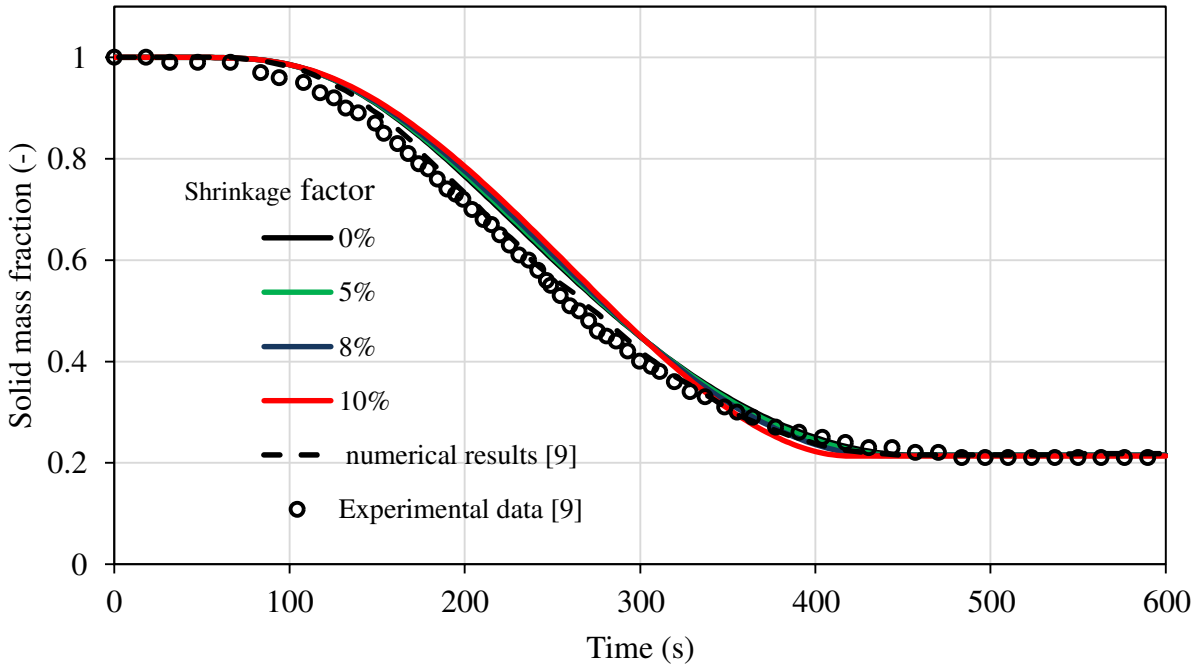


Fig. 5 Temporal evolution of normalized solid mass fraction using the char specific heat capacity correlation from [9].

3.6 Char yield and product distribution

The predicted char yield (Fig. 6) exhibits a slight but systematic decrease with increasing shrinkage. The model indicates a reduction from approximately 21.50 wt% at zero shrinkage to 21.32 wt% at a shrinkage factor of 0.10, improving agreement with the experimental value of 21.25 wt% reported in [9]. This behavior is attributed to the progressive reduction in volatile residence time within the particle as shrinkage proceeds, which slightly suppresses secondary char forming reactions [15]. The observed trend is consistent with findings reported in [32]. From a process perspective, even modest variations in predicted char yield may influence overall carbon conversion, downstream gas composition, and bio-oil recovery.

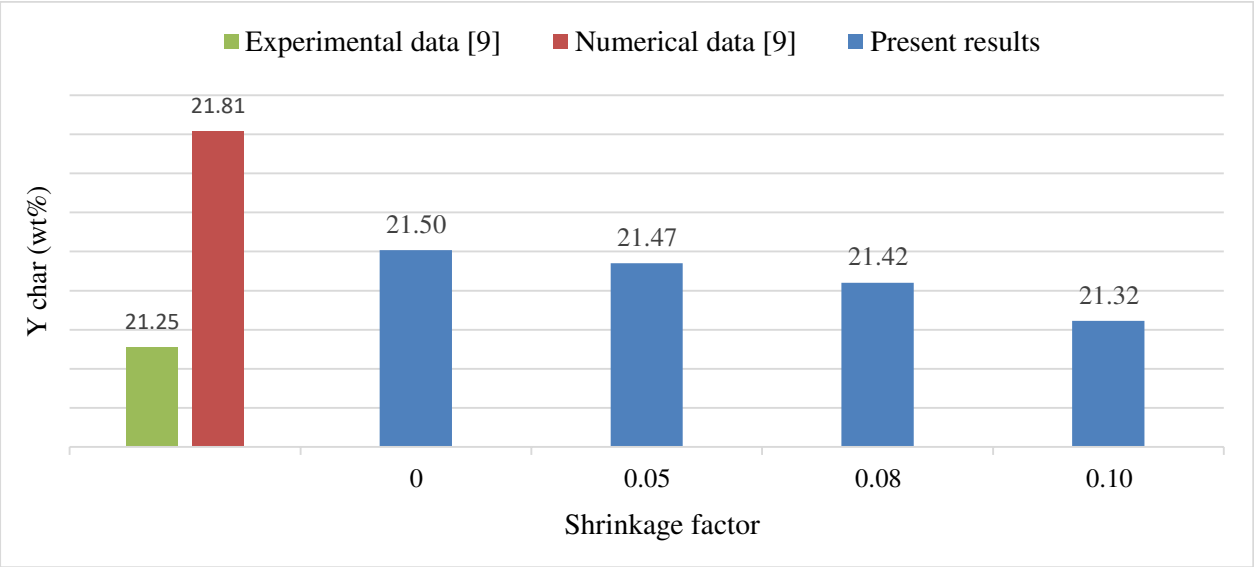


Fig. 6 Comparison of char yields for different shrinkage factors with numerical and experimental results from [9].

3.7 Internal fields and process coupling

The spatial distributions of temperature, pressure, and velocity, illustrated in Fig. 7, provide further insight into the internal dynamics of the particle. At early times, the temperature field exhibits strong radial gradients, confirming conduction dominated heat transfer [30, 49]. As devolatilization progresses, volatile generation increases internal pressure and induces outward gas flow. The interaction between thermal and flow fields becomes particularly pronounced during the intermediate stage, where the reaction front, pressure gradients, and velocity field develop simultaneously.

At later times, the exothermic decomposition of the intermediate solid leads to the formation of a localized high temperature region near the particle center, corresponding to the observed temperature maxima. This confirms that the temperature peak results from the coupling between heat generation and transport limitations rather than from purely conductive heating. Once the reactions are completed, the internal fields progressively relax toward equilibrium [9, 26, 30, 32].

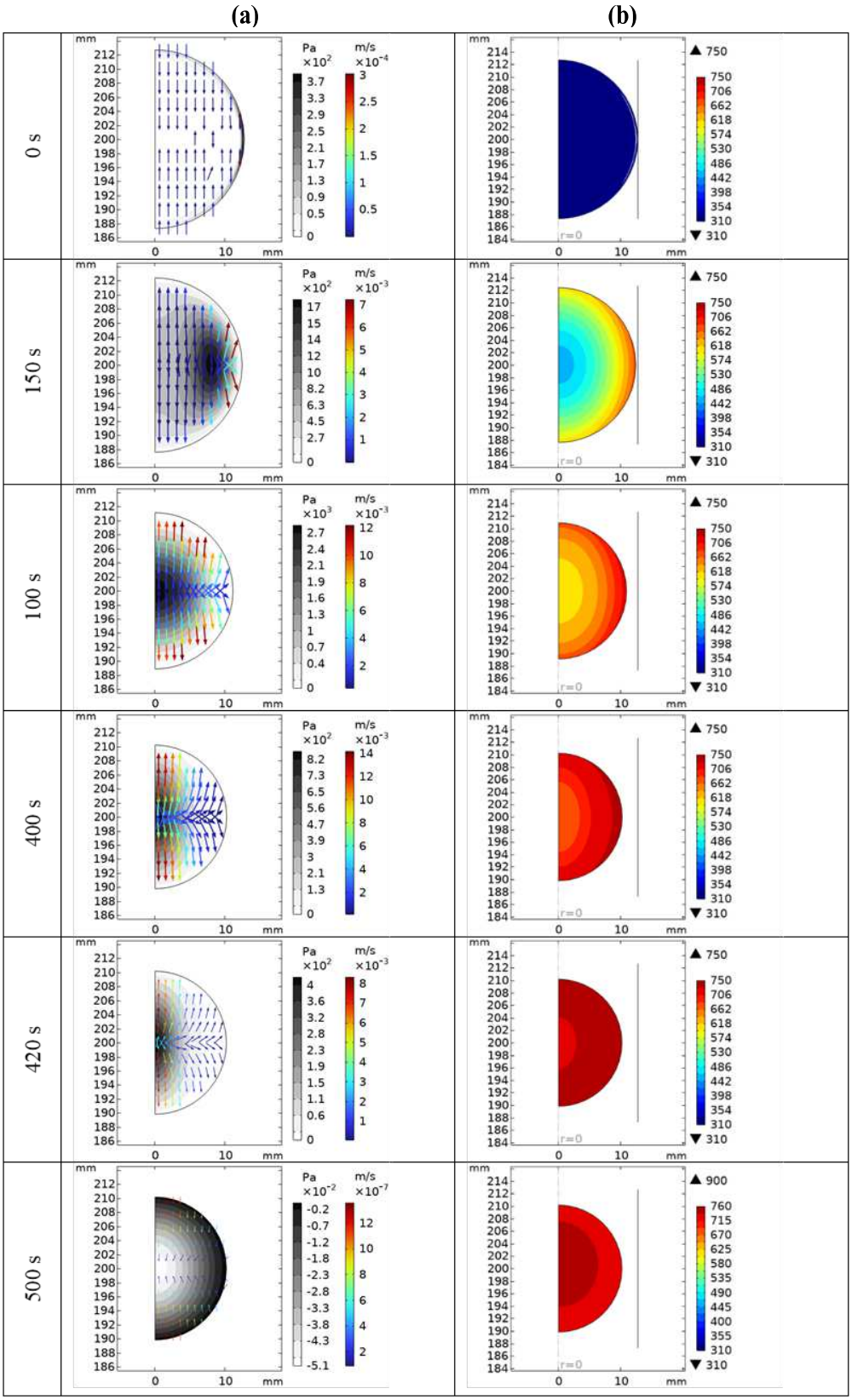


Fig. 7 Temporal evolution of (a) velocity and pressure fields, (b) temperature fields during a spherical particle pyrolysis for a 10% shrinkage factor using the char heat capacity correlation from [18].

3.8 Overall assessment

The present computational results demonstrate that the pyrolysis process of thermally thick biomass particles is governed by a strong coupling between heat transfer, reaction kinetics, and mass transport. The analysis highlights the significant influence of char heat capacity in controlling both the endothermic plateau and the exothermic temperature peak. Particle shrinkage, although having a limited effect on conversion time, significantly affects the thermal response and product yields through its impact on geometry and transport distances. The inclusion of anisotropic transport properties further improves the predictive capability of the model.

Under the present conditions, the combination of the linear temperature dependent char heat capacity proposed by [18] and a shrinkage factor of approximately 10% provide the most consistent agreement with experimental observations. Overall, accurate prediction of thermally thick pyrolysis requires a coupled description of temperature dependent wood biomass properties, geometry, and transport processes.

4. Conclusion

A transient two-dimensional multiphysics model was developed to investigate the pyrolysis of a 25.4 mm wood sphere under thermally thick conditions at a reactor wall temperature of 736 K. The model combines the intermediate solid kinetic scheme, anisotropic transport properties, particle shrinkage, and Darcy type volatile flow.

The simulations reproduced the characteristic thermal sequence of conductive heating and endothermic plateau, followed by an exothermic center temperature peak. These features are due to the kinetic mechanism, whereas thermophysical properties control their magnitude and timing. The choice of char heat capacity correlation significantly affects the predicted peak temperature, with differences of about 30–35 K among the tested formulations. The linear correlation [18] provides the closest agreement with published experimental data.

Particle shrinkage has a limited influence on overall conversion time but strongly affects internal heat transfer, peak temperature, and plateau duration. An optimal radial shrinkage of approximately 10% is identified, while larger values produce unrealistic thermal responses due to excessive reduction of the effective conduction length scale. The derived correlations for peak temperature and peak time provide a practical basis for estimating conversion dynamics.

Predicted char yields were only weakly influenced by shrinkage and heat capacity formulation, remaining close to reported experimental values. This indicates that, under the present thermally thick conditions, global mass conversion is lined mainly by heat transfer limitations, whereas kinetic and thermophysical parameters determine the internal thermal response.

Overall, the results demonstrate that reliable simulation of large biomass particles requires consistent treatment of structural evolution and anisotropic transport properties. Future work should extend the approach to packed beds and reactor scale systems, including detailed radiative heat transfer.

Funding

The authors declare that no funding, grants, or other financial support were received for this work.

Data Availability

The datasets generated during and/or analyzed during the current study are not publicly available but are available from the corresponding author upon reasonable request.

Declarations

Conflict of interest

The authors declare that they have no known competing financial or non-financial interests.

.

References

[1] Di Blasi, C.: Modeling chemical and physical processes of wood and biomass pyrolysis. Progress in Energy and Combustion Science 34, 47–90 (2008). https://doi.org/10.1016/j.pecs.2006.12.001

[2] Maziarka, P., Anca-Couce, A., Prins, W., Ronsse, F.: A meta-analysis of thermo-physical and chemical aspects in CFD modelling of pyrolysis of a single wood particle in the thermally thick regime. Chemical Engineering Journal 446, (2022). https://doi.org/10.1016/j.cej.2022.137088

[3] Karczewska, S.P., Hercel, P., Adibimanesh, B., Wardach-Święcicka, I.: Towards sustainable biomass conversion technologies: A review of mathematical modeling approaches. Sustainability 16, (2024). https://doi.org/10.3390/su16198719

[4] Mazza, G.D., Soria, J.M., Gauthier, D., Urrutia, A.R., Zambon, M., Flamant, G.: Environmentally friendly fluidized bed combustion of solid fuels: A review about local scale modeling of char heterogeneous combustion. Waste and Biomass Valorization 7, 237–266 (2016). https://doi.org/10.1007/s12649-015-9461-5

[5] Kansa, E.J., Perlee, H.E., Chaiken, R.F.: Mathematical model of wood pyrolysis including internal forced convection. Combustion and Flame 29, 311–324 (1977). https://doi.org/10.1016/0010-2180(77)90121-3

[6] Koufopanos, C.A., Papayannakos, N., Maschio, G., Lucchesi, A.: Modelling of the pyrolysis of biomass particles: Studies on kinetics, thermal and heat transfer effects. Canadian Journal of Chemical Engineering 69, 907–915 (1991). https://doi.org/10.1002/cjce.5450690413

[7] Pyle, L., Zaror, C.A.: Heat transfer and kinetics in the low temperature pyrolysis of solids. Chemical Engineering Science 39, 147–158 (1984). https://doi.org/10.1016/0009-2509(84)80140-2

[8] Gronli, M.G., Melaaen, M.C.: Mathematical model for wood pyrolysis comparison of experimental measurements with model predictions. Energy & Fuels 14, 791–800 (2000). https://doi.org/10.1021/ef990176q

[9] Park, W.C., Atreya, A., Baum, H.R.: Experimental and theoretical investigation of heat and mass transfer processes during wood pyrolysis. Combustion and Flame 157, 481–494 (2010). https://doi.org/10.1016/j.combustflame.2009.10.006

[10] Sadhukhan, A.K., Gupta, P., Saha, R.K.: Modelling and experimental studies on pyrolysis of biomass particles. Journal of Analytical and Applied Pyrolysis 81, 183–192 (2008). https://doi.org/10.1016/j.jaap.2007.11.007

[11] Sadhukhan, A.K., Gupta, P., Saha, R.K.: Modeling of pyrolysis of large wood particles. Bioresource Technology 100, 3134–3139 (2009). https://doi.org/10.1016/j.biortech.2009.01.007

[12] Corbetta, M., Frassoldati, A., Bennadji, H., Smith, K., Serapiglia, M.J., Gauthier, G., Melkior, T., Ranzi, E., Fisher, E.M.: Pyrolysis of centimeter-scale woody biomass particles: kinetic modeling and experimental validation. Energy & Fuels 28, 3884–3898 (2014). https://doi.org/10.1021/ef500525v

[13] Di Blasi, C.: Heat, momentum and mass transport through a shrinking biomass particle exposed to thermal radiation. Chemical Engineering Science 51, 1121–1132 (1996). https://doi.org/10.1016/S0009-2509(96)80011-X

[14] Bryden, K.M., Ragland, K.W., Rutland, C.J.: Modeling thermally thick pyrolysis of wood. Biomass and Bioenergy 22, 41–53 (2002). https://doi.org/10.1016/S0961-9534(01)00060-5

[15] Bryden, K.M., Hagge, M.J.: Modeling the combined impact of moisture and char shrinkage on the pyrolysis of a biomass particle. Fuel 82, 1633–1644 (2003). https://doi.org/10.1016/S0016-2361(03)00108-X

[16] Hagge, M.J., Bryden, K.M.: Modeling the impact of shrinkage on the pyrolysis of dry biomass. Chemical Engineering Science 57, 2811–2823 (2002). https://doi.org/10.1016/S0009-2509(02)00167-7

[17] Bellais, M., Davidsson, K.O., Liliedahl, T., Sjöström, K., Pettersson, J.B.C.: Pyrolysis of large wood particles: a study of shrinkage importance in simulations. Fuel 82, 1541–1548 (2003). https://doi.org/10.1016/S0016-2361(03)00062-0

[18] Babu, B.V., Chaurasia, A.S.: Heat transfer and kinetics in the pyrolysis of shrinking biomass particle. Chemical Engineering Science 59, 1999–2012 (2004). https://doi.org/10.1016/j.ces.2004.01.050

[19] Chaurasia, A.S., Kulkarni, B.D.: Most sensitive parameters in pyrolysis of shrinking biomass particle. Energy Conversion and Management 48, 836–849 (2007). https://doi.org/10.1016/j.enconman.2006.08.018

[20] Paulauskas, R., Džiugys, A., Striūgas, N.: Experimental investigation of wood pellet swelling and shrinking during pyrolysis. Fuel 142, 145–151 (2014). https://doi.org/10.1016/j.fuel.2014.11.023

[21] Thoharudin, T.: CFD simulation of biomass pyrolysis in a fluidized bed reactor: effect of particle shrinkage model. Formosa Journal of Science and Technology 3, 899–916 (2024). https://doi.org/10.55927/fjst.v3i5.9435

[22] Lu, H., Ip, E., Scott, J., Foster, P., Vickers, M., Baxter, L.L.: Effects of particle shape and size on devolatilization of biomass particle. Fuel 89, 1156–1168 (2010). https://doi.org/10.1016/j.fuel.2008.10.023

[23] Suriapparao, D.V., Vinu, R.: Effects of biomass particle size on slow pyrolysis kinetics and fast pyrolysis product distribution. Waste and Biomass Valorization 9, 465–477 (2018). https://doi.org/10.1007/s12649-016-9815-7

[24] Park, W.C.: A study of pyrolysis of charring materials and its application to fire safety and biomass utilization, Ph.D. dissertation, University of Michigan, USA (2008).

[25] Siau, J.F.: Transport processes in wood. Springer-Verlag, Berlin Heidelberg (1984).

[26] Di Blasi, C.: Physico-chemical processes occurring inside a degrading two-dimensional anisotropic porous medium. International Journal of Heat and Mass Transfer 41, 4139–4150 (1998). https://doi.org/10.1016/S0017-9310(98)00142-2

[27] Pecha, M.B., Thornburg, N.E., Peterson, C.A., Crowley, M.F., Gao, X., Lu, L., Wiggins, G., Brown, R.C., Ciesielski, P.N.: Impacts of anisotropic porosity on heat transfer and off-gassing during biomass pyrolysis. Energy & Fuels 35, 20131–20141 (2021). https://doi.org/10.1021/acs.energyfuels.1c02679

[28] Sánchez, M., Maya, J.C., Pecha, B., Chejne, F., Quinchía-Figueroa, A.M.: Effect of particle characteristics, kinetics and transport phenomena on the prediction of particle mass loss and products yields during biomass fast pyrolysis. Journal of Analytical and Applied Pyrolysis 168, (2022). https://doi.org/10.1016/j.jaap.2022.105786

[29] Blondeau, J., Jeanmart, H.: Biomass pyrolysis at high temperatures: Prediction of gaseous species yields from an anisotropic particle. Biomass and Bioenergy 41, 107–121 (2012). https://doi.org/10.1016/j.biombioe.2012.02.016

[30] Hercel, P., Orhon, A., Jóźwik, M., Kardaś, D.: 2D model of a biomass single particle pyrolysis—Analysis of the influence of fiber orientation on the thermal decomposition process. Sustainability 17, (2025). https://doi.org/10.3390/su17010279

[31] Martí-Rosselló, T., Li, J., Lue, L., Karlström, O., Brink, A.: Comprehensive assessment of particle-scale modeling for biomass pyrolysis: one-dimensional versus three-dimensional models. Energy & Fuels 35, 9937–9949 (2021). https://doi.org/10.1021/acs.energyfuels.1c00283

[32] Shi, X., Ronsse, F., Pieters, J.G.: Finite element modeling of intraparticle heterogeneous tar conversion during pyrolysis of woody biomass particles. Fuel Processing Technology 148, 302–316 (2016). https://doi.org/10.1016/j.fuproc.2016.03.010

[33] Caposciutti, G., Almuina-Villar, H., Dieguez-Alonso, A., Gruber, T., Kelz, J., Desideri, U., Hochenauer, C., Scharler, R., Anca-Couce, A.: Experimental investigation on biomass shrinking and swelling behaviour: particles pyrolysis and wood logs combustion. Biomass and Bioenergy 123, 1–13 (2019). https://doi.org/10.1016/j.biombioe.2019.01.044

[34] Pattanotai, T., Watanabe, H., Okazaki, K.: Gasification characteristic of large wood chars with anisotropic structure. Fuel 117, 331–339 (2014). https://doi.org/10.1016/j.fuel.2013.09.030

[35] Flity, H., Abdo, M., Terrei, L., Acem, Z., Mehaddi, R., Lardet, P., Parent, G.: 3D-Modeling of thermal degradation of spruce wood under inert atmosphere. Fire Safety Journal 141, (2023). https://doi.org/10.1016/j.firesaf.2023.103979

[36] Flity, H., Jannot, Y., Terrei, L., Lardet, P., Schick, V., Acem, Z., Parent, G.: Thermal conductivity parallel and perpendicular to fibers direction and heat capacity measurements of eight wood species up to 160 °C. International Journal of Thermal Sciences 195, (2024). https://doi.org/10.1016/j.ijthermalsci.2023.108661

[37] Dsouza, R.D., Harjupatana, T., Miettinen, A., Brandstätter, F., Harju, A., Venäläinen, M., Möttönen, V., Borrega, M., Paajanen, A., Füssel, J., Fortino, S.: Multi-phase model for moisture transport in wood supported by X-ray computed tomography data. Wood Science and Technology 59, 1–28 (2025). https://doi.org/10.1007/s00226-025-01635-9

[38] Anca-Couce, A.: Reaction mechanisms and multi-scale modelling of lignocellulosic biomass pyrolysis. Progress in Energy and Combustion Science 53, 41–79 (2016). https://doi.org/10.1016/j.pecs.2015.10.002

[39] Gao, X., Lu, L., Shahnam, M., Rogers, W.A., Smith, K., Gaston, K., Robichaud, D., Pecha, M.B., Crowley, M., Ciesielski, P.N., Debiagi, P., Faravelli, T., Wiggins, G., Finney, C.E.A., Parks II, J.E.: Assessment of a detailed biomass pyrolysis kinetic scheme in multiscale simulations of a single-particle pyrolyzer and a pilot-scale entrained flow pyrolyzer. Chemical Engineering Journal 418, (2021). https://doi.org/10.1016/j.cej.2021.129347

[40] Kple, M., Girods, P., Fagla, B., Anjorin, M., Ziegler-Devin, I., Rogaume, Y.: Kinetic study of low density polyethylene using thermogravimetric analysis, part 2: Isothermal study. Waste and Biomass Valorization 8, 707–719 (2017). https://doi.org/10.1007/s12649-016-9590-5

[41] Ranzi, E., Debiagi, P.E.A., Frassoldati, A.: Mathematical modeling of fast biomass pyrolysis and bio-oil formation. Note I: Kinetic mechanism of biomass pyrolysis. ACS Sustainable Chemistry & Engineering 5, 2867–2881 (2017). https://doi.org/10.1021/acssuschemeng.6b03096

[42] Han, F.-y., Wang, M., Ma, X.-b., Yin, L.-j., Chen, D.-z., Liu, Z.-q., Zhang, R.-n.: Numerical simulation of heat transfer properties of large-sized biomass particles during pyrolysis process. Heliyon 9, (2023). https://doi.org/10.1016/j.heliyon.2023.e21255

[43] Babu, B.V., Chaurasia, A.S.: Modeling for pyrolysis of solid particle: Kinetics and heat transfer effects. Energy Conversion and Management 44, 2251–2275 (2003). https://doi.org/10.1016/S0196-8904(02)00252-2

[44] Kaczor, Z., Buliński, Z., Werle, S.: Modelling approaches to waste biomass pyrolysis: a review. Renewable Energy 159, 427–443 (2020). https://doi.org/10.1016/j.renene.2020.05.110

[45] Kortas, S., Méchi, R., Farhat, H., Halouani, K.: Impact of operating parameters on biomass pyrolysis in a fluidized bed reactor. In the proceedings of 15th International Renewable Energy Congress (IREC), Hammamet, Tunisia (2025). https://doi.org/10.1109/IREC64614.2025.10926789

[46] Sharma, A.K.: Equilibrium and kinetic modeling of char reduction reactions in a downdraft biomass gasifier: A comparison. Solar Energy 82, 918–928 (2008). https://doi.org/10.1016/j.solener.2008.03.004

[47] Bennadji, H., Smith, K., Serapiglia, M.J., Fisher, E.M.: Effect of particle size on low-temperature pyrolysis of woody biomass. Energy & Fuels 28, 7527–7537 (2014). https://doi.org/10.1021/ef501869e

[48] Ciesielski, P.N., Wiggins, G.M., Jakes, J.E., Daw, C.S.: Simulating biomass fast pyrolysis at the single particle scale. In: Fast Pyrolysis of Biomass: Advances in Science and Technology, Green Chemistry Series, chapter 11, pp. 231–253. (2017). https://doi.org/10.1039/9781788010245-00231

[49] Di Blasi, C.: Modeling intra- and extra-particle processes of wood fast pyrolysis. AIChE Journal 48, 2386–2397 (2002). https://doi.org/10.1002/aic.690481028